Geomechanics and Engineering, *Vol. 19, No. 1 (2019) 61-70*
DOI: https://doi.org/10.12989/gae.2019.19.1.061

Mechanical analysis of tunnels supported by yieldable steel ribs in rheological rocks

Kui Wu[a], Zhushan Shao*, Su Qin[b] and Nannan Zhao[c]

School of Civil Engineering, Xi'an University of Architecture & Technology, Xi'an 710055, China

(Received December 26, 2018, Revised August 29, 2019, Accepted September 6, 2019)

Abstract. Yieldable steel ribs have been widely applied in tunnels excavated in rheological rocks. For further understanding the influence of yieldable steel ribs on supporting effect, mechanical behavior of tunnels supported by them in rheological rocks is investigated in this paper. Taking into account the deformation characteristic of yieldable steel ribs, their deformation is divided into three stages. In order to modify the stiffness of yieldable steel ribs in different deformation stages, two stiffness correction factors are introduced in the latter two stages. Viscoelastic analytical solutions for the displacement and pressure in the rock-support interface in each deformation stage are obtained. The reliability of the theoretical analysis is verified by use of numerical simulation. It could be concluded that yieldable steel ribs are able to reduce pressure acting on them without becoming damaged through accommodating the rock deformation. The influence of stiffness correction factor in yielding deformation stage on pressure and displacement could be neglected with it remaining at a low level. Furthermore, there is a linearly descending relationship of pressure with yielding displacement in linear viscoelastic rocks.

Keywords: tunnel; viscoelasticity; yieldable steel ribs; analytical solution; support parameters

1. Introduction

With the rapid development of transportation infrastructure and underground space utilization, tunnels have been found to be widely used for many specific purposes (Lai *et al.* 2018, Wu *et al.* 2018, 2019, Qiao *et al.* 2018, 2019). Recently, more and more tunnels are being constructed or planned to be excavated in various complex geological conditions, including rheological soft rock mass (Shin *et al.* 2011, Sharifzadeh *et al.* 2013, Wang and Huang 2014, Fan *et al.* 2017, Qiu *et al.* 2018, Yang *et al.* 2018, Zhao *et al.* 2018). However, many researches show that the problem of large deformation and support failure is prone to occur when tunnels are driven in this stratum.

In the past decades, many researchers have tried to solve such problem by use of various methods (Shin *et al.* 2011, Kong *et al.* 2016, Sharifzadeh *et al.* 2012, Lee 2016, Zhou *et al.* 2016, Huang *et al.* 2017, Hu *et al.* 2018). Yang *et al.* (2017) proposed a new "bolt-cable-mesh-shotcrete + shell" combined support after analysis of failure process of roadway. Ding (2018) investigated the influence of tunnel burial depth, tunnel diameter and lateral pressure coefficient of original rock stress on the stress and deformation of tunnel surrounding rock. However, many studies indicated that the only feasible solution in heavily rheological soft rock mass is a tunnel support that is able to deform without becoming damaged-that is so-called "yielding supports", in combination with a certain amount of over-excavation in order to accommodate the deformations (Cantieni and Anagnostou 2009, Wu and Shao 2019a). The idea behind all these support structures is that the ground pressure will decrease if the ground is allowed to deform. Many researchers have performed the deep studies on these supports and also developed some new structures (Schubert 1996, Tian *et al.* 2016, 2018, Wang *et al.* 2017, Mezger *et al.* 2018, Wu and Shao 2019b). As a type of yielding supports, yieldable steel ribs, as shown in Fig. 1, are often recommended if tunnels are driven in rheological rocks. Jiang *et al.* (2011) calculated the internal forces of a close type yieldable steel support and Li *et al.* (2017) performed an experimental study on bearing capacity of it. You (2002) analyzed the effect of the support overlap parts on the stability of steel ribs. Jiao *et al.* (2013) improved the traditional yieldable structure and successfully used it for supporting tunnels in loose thick coal seam. The aforementioned works could provide useful guidance for support design. However, there are few closed analytical solutions for mechanical behavior of tunnels supported by yieldable steel ribs in recent literature.

For better understanding of mechanical behavior of tunnels supported by yieldable steel ribs in rheological rocks, a theoretical analysis is performed in this paper. Taking into account the deformation characteristics of yieldable steel ribs, their deformation is divided into three stages and support stiffness correction is carried out in different stages. Closed form solutions for the displacement in rock/support interface and for the pressure exerted by

*Corresponding author, Professor
E-mail: shaozhushan@xauat.edu.cn
[a]Ph.D. Student
E-mail: wukuigz@163.com
[b]Ph.D. Student
E-mail: qinsxauat@126.com
[c]Ph.D. Student
E-mail: zhaonannan0008@163.com

http://www.techno-press.org/?journal=gae&subpage=7
ISSN: 2005-307X (Print), 2092-6219 (Online)

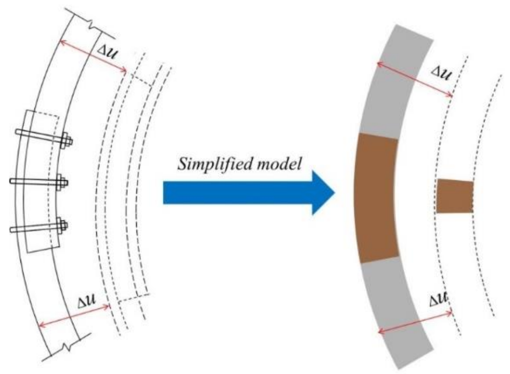

Fig. 1 Sketch of yieldable steel ribs

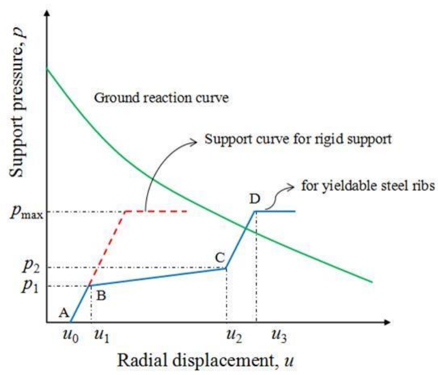

Fig. 2 Support characteristic curve for yieldable steel ribs and non-deformable arch

rock deformation on the support in different stages are provided. In addition, the effectiveness and reliability of theoretical analysis is verified by use of finite element method (FEM). Furthermore, based on the analytical solutions provided, the investigation on the effect of parameters of yieldable steel ribs on supporting effect is conducted. The results in the paper can provide some useful guidance for the design of similar projects.

2. Definition of the problem

Basically, joints of yieldable steel ribs would be allowed to slide if pressure on them exceeds a certain threshold, which causes different support characteristic curves for yieldable steel ribs and rigid support. As shown in Fig. 2, based on the deformation behavior of yieldable steel rib, support characteristic curve for them could be divided into four different parts as follows:

AB: In the early stage, joints of yieldable steel ribs fail to slide since pressure on them has not reached yielding pressure p_1. At this stage, support only generates small elastic displacement u_1-u_0.

BC: With the gradually increasing pressure on yieldable steel ribs, it has reached the predetermined threshold p_1 and joints begin to slide in this stage. During the movement of overlap parts of joints, the radius of the support continues to decrease. Instead the overlapping length of joints gradually increases until length designed runs out. In this stage, pressure-displacement curve displays a small slope between (u_1, p_1) and (u_2, p_2). Deformation of support structure at this stage could be regarded as yielding deformation.

CD: If shrinkage provided by joints runs out, joints are not allowed to slide any more and yieldable steel ribs enter a new deformation stage again. In this stage, deformation could also be seen as elastic part.

When load on yieldable steel ribs reaches support capacity p_{max}, it would cause buckling deformation and failure of yieldable steel ribs, which is beyond the scope of this paper.

In this paper, the problem deals with a circular reinforced hole supported by yieldable steel ribs in rheological rocks. To simplify the theoretical derivation, the following assumptions are made:

(a) Rock is homogeneous, isotropic, and exhibits linearly viscoelastic property.

(b) The initial state of ground stress is hydrostatic.

(c) The deformation of yieldable steel ribs is classified as first part of elastic deformation, second part of yielding deformation and third part of elastic deformation.

3. Constitutive model of rock

It is well know that it is an effective method to use physical model to describe the time-dependent behavior of geomaterials. For viscoelastic geomaterials, the rheological model could be represented by several springs and dashpots connected either in parallel or series.

As illustrated in Fig. 3(a), Maxwell model is formed by a spring and a dashpot connected in series. Once by a constant stress immediately, the Maxwell model displays an instantaneous elastic strain firstly and then a steadily increasing and irreversible creep behavior follows. Instead, Kelvin model is made up of a spring and a dashpot connected in parallel (see Fig. 3(b)). Under an instantly applied constant load, the strain increases asymptotically to its final value.

In Fig. 3(c), Maxwell model connected in series with Kelvin model is in the formation of the linearly viscoelastic

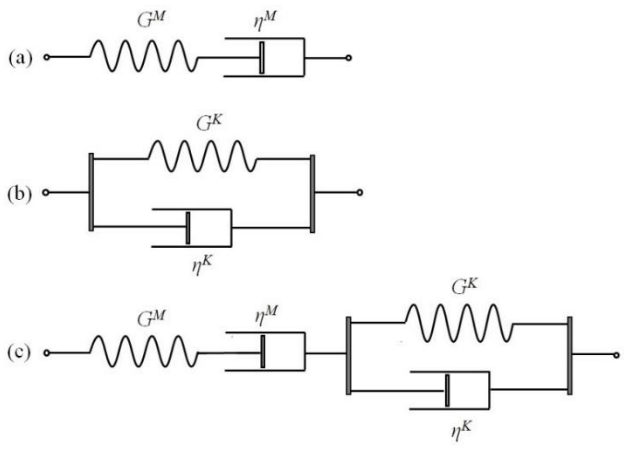

Fig. 3 Physical model (a) Maxwell model, (b) Kelvin model and (c) Burgers model

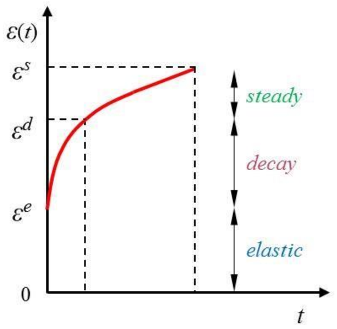

Fig. 4 Characteristic curve for creep behavior of Burgers model

Table 1 Coefficients of A_k and B_k

k	2	1	0
A_k	1	$G^M/\eta^M+G^M/\eta^K+G^K/\eta^K$	$G^MG^K/\eta^M\eta^K$
B_k	$2G^M$	$2G^MG^K/\eta^K$	0

Burgers model. According to Goodman (1989), Burgers model is preferable for engineering purposes. As shown in Fig. 4, once by an immediate load, the Burgers model firstly exhibits an elastic strain and then the decay and steady creep behavior could also be traced. Moreover, only four deformation parameters are involved in Burgers model, i.e., G^M, η^M, G^K and η^K, which could have been given less attention to run parametric investigation.

According to the composition of Burgers model, its deviatoric stress and strain could be calculated as

$$\begin{cases} s_{ij} = s_{ij}^M = s_{ij}^K \\ e_{ij} = e_{ij}^K + e_{ij}^M \end{cases} \tag{1}$$

where s_{ij} and e_{ij} denote tensors of stress and strain deviators, respectively. The superscripts M and K represent the Maxwell and Kelvin components of the corresponding variables.

In general, the constitutive equations of Maxwell and Kelvin model could be expressed as

$$\dot{e}_{ij}^M = \frac{s_{ij}^M}{2\eta^M} + \frac{\dot{s}_{ij}^M}{2G^M} \tag{2}$$

$$s_{ij}^K = 2G^K e_{ij}^K + 2\eta^K \dot{e}_{ij}^K \tag{3}$$

with the overdot denoting the time derivative. G and η are spring constant and viscosity coefficient of dashpot, respectively.

Then, substituting the Eqs. (2) and (3) into Eq. (1) yields the constitutive equation of Burgers model as follows

$$\ddot{s}_{ij} + \left(\frac{G^M}{\eta^M} + \frac{G^M}{\eta^K} + \frac{G^K}{\eta^K}\right)\dot{s}_{ij} + \left(\frac{G^M G^K}{\eta^M \eta^K}\right)s_{ij} = 2G^M \ddot{e}_{ij} + 2\frac{G^M G^K}{\eta^K}\dot{e}_{ij} \tag{4}$$

For simplification of theoretical derivation, it is useful to use the linear differential time operators Q and P to rewrite the linear viscoelastic constitutive equation of Burgers model. Thus, the Eq. (4) can be re-expressed as

$$Qs_{ij} = Pe_{ij} \tag{5}$$

with Q and P as follows

$$Q = \sum_0^2 A_k \frac{d^k}{dt^k}, \quad P = \sum_0^2 B_k \frac{d^k}{dt^k} \tag{6}$$

in which A_k and B_k are listed in Table 1, respectively.

In cylindrical coordinates, Eq. (5) in r, θ, z would be converted

$$Q(\sigma_r - \sigma_{mean}) = P(\varepsilon_r - \varepsilon_{mean}) \tag{7}$$

$$Q(\sigma_\theta - \sigma_{mean}) = P(\varepsilon_\theta - \varepsilon_{mean}) \tag{8}$$

$$Q(\sigma_z - \sigma_{mean}) = P(\varepsilon_z - \varepsilon_{mean}) \tag{9}$$

where σ_r, σ_θ and σ_z represent radial, tangential and axial stress, respectively. ε_r, ε_θ and ε_z denote radial, tangential and axial strain, respectively. σ_{mean} and ε_{mean} are the mean stress and strain, respectively, computed as

$$\begin{cases} \sigma_{mean} = \dfrac{\sigma_r + \sigma_\theta + \sigma_r}{3} \\ \varepsilon_{mean} = \dfrac{\varepsilon_r + \varepsilon_\theta + \varepsilon_r}{3} \end{cases} \tag{10}$$

4. Theoretical derivation

4.1 Fundamental formula

As illustrated in Fig. 5, based on the theory of elasticity, the stress field around an axisymmetric pressure hole is available. By use of correspondence principle, for the viscoelastic plane strain problem stress field could be expressed as

$$\begin{cases} \sigma_r = \left(1 - \dfrac{R^2}{r^2}\right)p_0 + \dfrac{R^2}{r^2}p(t) \\ \varepsilon_\theta = \left(1 + \dfrac{R^2}{r^2}\right)p_0 - \dfrac{R^2}{r^2}p(t) \end{cases} \tag{11}$$

where p_0 represents uniform stress at infinity and $p(t)$ is internal pressure. R and r are the hole radius and the distance between element studied and hole center point, respectively.

Based on the Eq. (11), the deviatoric stress field around this opening could be calculated as

$$\begin{cases} \Delta\sigma_r = \left[-p_0 + p(t)\right]\dfrac{R^2}{r^2} \\ \Delta\sigma_\theta = \left[p_0 - p(t)\right]\dfrac{R^2}{r^2} \end{cases} \tag{12}$$

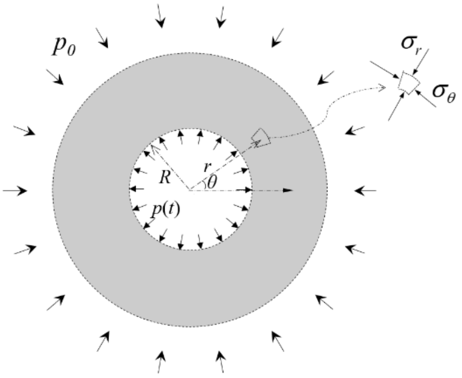

Fig. 5 Mechanical model of axisymmetric pressure hole

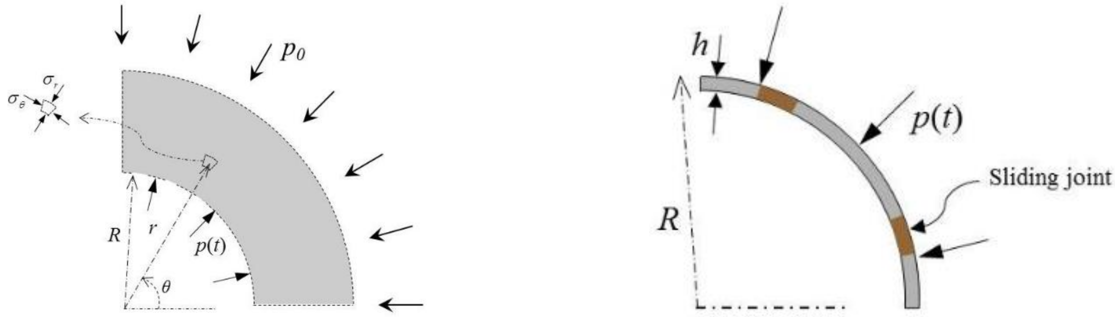

(a) Rock (b) Yieldable steel ribs

Fig. 6 Illustration of tunnel mechanical model

with $\Delta\sigma_r$ and $\Delta\sigma_\theta$ being the radial and tangential deviatoric stresses, respectively.

Thus, substituting r=R into the Eq. (12) yields the radial and tangential deviatoric stresses at the tunnel wall as follows

$$\begin{cases} \Delta\sigma_r = -p_0 + p(t) \\ \Delta\sigma_\theta = p_0 - p(t) \end{cases} \tag{13}$$

Based on the displacement-strain relation, the tangential strain difference could be written as

$$\Delta\varepsilon_\theta = u(r,t)/r \tag{14}$$

in which $\Delta\varepsilon_\theta$ represents tangential deviatoric strain and $u(r;t)$ denotes radial displacement.

Similarly, at the tunnel wall, i.e., r=R, Eq. (14) becomes

$$\Delta\varepsilon_\theta = u_R(t)/R \tag{15}$$

where $u_R(t)$ is the radial displacement of the wall.

4.2 First part of elastic deformation

As mentioned above, in the first part of elastic deformation, pressure acting on the yieldable steel ribs has not reached yielding pressure p_1 and thus joints fail to slide.

When the yieldable steel ribs are installed at time t=0, as shown in Fig. 6, the pressure acting on the support (also reaction force of support on rock) could be calculated as

$$p(t) = K_S \frac{u_R(t) - u_R(0)}{R} \tag{16}$$

with K_S being the stiffness of yieldable steel ribs in the first part of elastic deformation.

By Substituting Eq. (16) into Eq. (13), the tangential deviatoric stress at the tunnel wall could be calculated as

$$\Delta\sigma_\theta = p_0 - K_S \frac{u_R(t) - u_R(0)}{R} \tag{17}$$

Then substituting the Eqs. (15) and (17) into Eq. (8) provides the governing equation of displacement in the rock-support interface as follows

$$\sum_0^2 \left(B_k + K_S A_k\right) \frac{d^k}{dt^k} u_R(t) = A_0 \left[K_S u_R(0) + p_0 R\right] \tag{18}$$

Basically, two initial conditions are required in order to obtain the analytical solution for displacement in the rock-support interface by solving the Eq. (18). Based on the Eq. (18), one is the instantaneous deformation of unlined tunnel after excavation completed at t=0, which could be given by

$$u_R(0) = \frac{p_0 R}{2G^M} \tag{19}$$

According to the Eq. (18), the other initial condition should be the displacement rate at t=0 in the rock-support interface. Accounting for the interaction between rock and yieldable steel ribs after support installation, coordinate deformation between them needs to be satisfied and the initial displacement rate at t=0 could be calculated as

$$\dot{u}_R(0) = \frac{p_0 R}{2\left(1+K_S/2G^M\right)}\left(\frac{1}{\eta^M}+\frac{1}{\eta^K}\right) \tag{20}$$

Therefore, the linear differential equation (18) can be solved by the Eqs. (19) and (20) and the analytical solution in closed form for the displacement in the rock-support interface in the first part of elastic deformation could be given by

$$u_R(t) = \frac{p_0 R}{K_S}\left[\left(\frac{K_S}{2G^M}+1\right)+\frac{F_1 e^{a_1 t}-F_2 e^{a_2 t}}{a_1-a_2}\right] \tag{21}$$

where $a_{1,2}$ are the roots (both negative) of the following equation

$$a^2+\left[\frac{2G^M/K_S+G^M/G^K+T^K/T^M+1}{\left(2G^M/K_S+1\right)T^K T^M}\right]a+\left[\frac{1}{\left(2G^M/K_S+1\right)T^K T^M}\right]=0 \tag{22}$$

with T^M and T^K being ratio of dashpot's viscosity coefficient to spring constant in Maxwell model and in Kelvin model. and F_1, F_2 are given by

$$F_1 = \frac{1+a_1 T^K\left(1+\eta^M/\eta^K\right)}{a_1\left(2G^M/K_S+1\right)T^K T^M} \tag{23}$$

$$F_2 = \frac{1+a_2 T^K\left(1+\eta^M/\eta^K\right)}{a_2\left(2G^M/K_S+1\right)T^K T^M} \tag{24}$$

Then, substituting the Eqs. (19) and (20) into Eq. (16) yields the pressure acting on yieldable steel ribs in the first stage as follows

$$p(t) = p_0\left(1+\frac{F_1 e^{a_1 t}-F_2 e^{a_2 t}}{a_1-a_2}\right) \tag{25}$$

Due to no slide of joints in the first part of elastic deformation, the pressure acting on the yieldable steel ribs has not reached yielding pressure p_1. The above theoretical analysis is only valid for the first part of elastic deformation from time 0 to t_1, i.e., $p(t)\le p_1$ and $u_R(t)\le u_1$.

4.3 Second part of yielding deformation

In the second part of yielding deformation, joints are allowed to slide since the pressure acting on yieldable steel ribs has reached the yielding pressure p_1. As illustrated in Fig. 2, the principle of pressure-displacement development in this stage is obviously distinct from that in the first part of elastic deformation. Because the support deformation is mainly caused by movement of joints in this stage, support stiffness of yieldable steel ribs has changed. In order to modify the support stiffness in this stage, stiffness correction factor λ_1 is introduced.

Then, in this deformation stage, pressure acting on support could be calculated as

$$p(t) = p_1+\lambda_1 K_S\frac{u_R(t)-u_1}{R} \tag{26}$$

Substituting the Eq. (26) into Eq. (13) provides the tangential deviatoric stress at the tunnel wall in the second part of yielding deformation as follows

$$\Delta\sigma_\theta = p_0-p_1-\lambda_1 K_S\frac{u_R(t)-u_1}{R} \tag{27}$$

By substituting the Eqs. (15) and (27) into Eq. (8), the governing equation of displacement in the rock-support interface in the second deformation part could be calculated as

$$\sum_0^2\left(B_k+\lambda_1 K_S A_k\right)\frac{d^k}{dt^k}u_R(t) = A_0\left[p_0 R-p_1 R+\lambda_1 K_S u_1\right] \tag{28}$$

Similarly, the analytical solution for displacement in the rock-support interface could be obtained by solving the Eq. (28), which requires two initial conditions as well. Based on the Eq. (21), the displacement at time t=t_1 could be given by

$$u_R(t_1) = \frac{p_0 R}{K_S}\left[\left(\frac{K_S}{2G^M}+1\right)+\frac{F_1 e^{a_1 t_1}-F_2 e^{a_2 t_1}}{a_1-a_2}\right]=u_1 \tag{29}$$

Because pressure acting on support has reached a certain threshold p_1 at time t=t_1, joints of yieldable steel ribs begin to slide, which leads to the sudden change of stiffness of the yieldable steel ribs. It is accepted that deformation coordination in the rock-support interface needs to be satisfied at any time. So based on the analysis on the deformation consistency in the rock-support interface, the displacement rate could be calculated at time t=t_1 as follows

$$\dot{u}_R(t_1) = \frac{p_0 R\left(F_1 a_1 e^{a_1 t_1}-F_2 a_2 e^{a_2 t_1}\right)}{K_S\left[1+\left(\lambda_1-1\right)K_S/2G^M\right]\left(a_1-a_2\right)} \tag{30}$$

Then solving the Eq. (28) by use of the Eqs. (29) and (30) provides the following analytical solution for displacement in the rock-support interface in the second part of yielding deformation.

$$u_R(t) = u_1+\frac{p_0 R-p_1 R}{\lambda_1 K_S}+\frac{F_3 e^{a_3(t-t_1)}-F_4 e^{a_4(t-t_1)}}{a_3-a_4} \tag{31}$$

with $a_{3,4}$ being the roots (both negative) of the following equation

$$a^2+\frac{2\eta^M/\lambda_1 K_S+\eta^M/G^K+T^M+T^K}{\left(1+2G^M/\lambda_1 K_S\right)T^M T^K}a+\frac{1}{\left(1+2G^M/\lambda_1 K_S\right)T^M T^K}=0 \tag{32}$$

and F_3, F_4 are given by

$$F_3 = \frac{p_0 R\left(F_1 a_1 e^{a_1 t_1}-F_2 a_2 e^{a_2 t_1}\right)}{K_S\left[1+\left(\lambda_1-1\right)K_S/2G^M\right]\left(a_1-a_2\right)}+a_4\frac{p_0 R-p_1 R}{\lambda_1 K_S} \tag{33}$$

$$F_4 = \frac{p_0 R\left(F_1 a_1 e^{a_1 t_1} - F_2 a_2 e^{a_2 t_1}\right)}{K_S\left[1+\left(\lambda_1 - 1\right)K_S / 2G^M\right]\left(a_1 - a_2\right)} + a_3 \frac{p_0 R - p_1 R}{\lambda_1 K_S} \quad (34)$$

So, by substituting the Eq. (31) into Eq. (27), pressure acting on the yieldable steel ribs could be calculated as

$$p(t) = p_0 + \frac{\lambda_1 K_S\left[F_3 e^{a_3(t-t_1)} - F_4 e^{a_4(t-t_1)}\right]}{R\left(a_3 - a_4\right)} \quad (35)$$

When shrinkage provided by joints has run out at time t=t_2, pressure acting on yieldable steel ribs and displacement would reach limit values in this stage, p_2 and u_2, respectively. Also, the analytical solutions for displacement and pressure above are only applicable to prediction in the second part of yielding deformation from time t_1 to t_2.

4.4 Third part of elastic deformation

From time t=t_2, joints would not be allowed to slide anymore and yieldable steel ribs begin to enter third part of elastic deformation. In this stage, stiffness correction factor λ_2 is introduced.

Then, the pressure acting on yieldable steel ribs in this stage becomes as

$$p(t) = p_2 + \lambda_2 K_S \frac{u_R(t) - u_2}{R} \quad (36)$$

Applying Eq. (36) into Eq. (13) yields the tangential deviatoric stress at tunnel wall as follows

$$\Delta\sigma_\theta = p_0 - p_2 - \lambda_2 K_S \frac{u_R(t) - u_2}{R} \quad (37)$$

By substituting the Eqs. (15) and (37) into Eq. (8), governing equation of displacement in the rock-support interface in the third part of elastic deformation could be expressed as

$$\sum_0^2\left(B_k + \lambda_2 K_S A_k\right)\frac{d^k}{dt^k}u_R(t) = A_0\left[p_0 R - P_2 R + \lambda_2 K_S u_2\right] \quad (38)$$

It is obvious that by use of Eq. (31) one initial condition for solving Eq. (38) could be given by

$$u_R(t_2) = u_1 + \frac{p_0 R - P_1 R}{\lambda_1 K_S} + \frac{F_3 e^{a_3(t_2-t_1)} - F_4 e^{a_4(t_2-t_1)}}{a_3 - a_4} = u_2 \quad (39)$$

At time t=t_2, shrinkage provided by joints has run out. With still increasing pressure, yieldable steel ribs begin to enter elastic deformation stage once again. There is also a sudden change in the stiffness of support at this time. In order to meet deformation coordination in the rock-support interface, the other initial condition for the displacement rate at time t=t_2 should be expressed as

$$\dot{u}_R(t_2) = \frac{F_3 a_3 e^{a_3(t_2-t_1)} - F_4 a_4 e^{a_4(t_2-t_1)}}{\left[1+\left(\lambda_2 - \lambda_1\right)K_S / 2G^M\right]\left(a_3 - a_4\right)} \quad (40)$$

The linear differential equation (38) can be solved by the Eqs. (39) and (40) and the displacement expression in the rock-support interface in the third part of elastic deformation could be given by

$$u_R(t) = u_2 + \frac{p_0 R - p_2 R}{\lambda_2 K_S} + \frac{F_5 e^{a_5(t-t_2)} - F_6 e^{a_6(t-t_2)}}{a_5 - a_6} \quad (41)$$

where $a_{5,6}$ are the roots (both negative) of the following equation

$$a^2 + \frac{2\eta^M / \lambda_2 K_S + \eta^M / G^K + T^M + T^K}{\left(1+2G^M / \lambda_2 K_S\right)T^M T^K}a + \frac{1}{\left(1+2G^M / \lambda_2 K_S\right)T^M T^K} = 0 \quad (42)$$

and F_5, F_6 are given by

$$F_5 = \frac{F_3 a_3 e^{a_3(t_2-t_1)} - F_4 a_4 e^{a_4(t_2-t_1)}}{\left[1+\left(\lambda_2 - \lambda_1\right)K_S / 2G^M\right]\left(a_3 - a_4\right)} + a_6 \frac{p_0 R - p_2 R}{\lambda_2 K_S} \quad (43)$$

$$F_6 = \frac{F_3 a_3 e^{a_3(t_2-t_1)} - F_4 a_4 e^{a_4(t_2-t_1)}}{\left[1+\left(\lambda_2 - \lambda_1\right)K_S / 2G^M\right]\left(a_3 - a_4\right)} + a_5 \frac{p_0 R - p_2 R}{\lambda_2 K_S} \quad (44)$$

By substituting Eq. (41) to Eq. (36), pressure acting on yieldable steel ribs in the third part of elastic deformation could be calculated as

$$p(t) = p_0 + \frac{\lambda_2 K_S\left[F_5 e^{a_5(t-t_2)} - F_6 e^{a_6(t-t_2)}\right]}{R\left(a_5 - a_6\right)} \quad (45)$$

With gradually increasing pressure acting on yieldable steel ribs, pressure would reach bearing capacity of yieldable steel ribs and failure inevitably occur during deformation. Therefore, the analytical solutions for displacement and pressure provided in the third part of elastic deformation would no longer applicable.

5. Results and discussion

5.1 Verification

In order to fully display the accuracy and reliability of the provided analytical solutions, the comparison is performed between theoretical and numerical (by use of ABAQUS software) results. The tunnel radius, in-situ stress, rock parameters and support properties applied in the calculation are taken from Goodman (1989), listed in Table 2, respectively. Noting that, in this calculation, parameters associated with support stiffness change are assumed that λ_1=0.1, λ_2=1.0, p_1=1MPa and p_2=1.6MPa.

As shown in Figs. 7 and 8, curves for pressure and radial displacement in the rock-support interface with time and the support characteristic curve are plotted, respectively. In the Figs. 7 and 8, the comparison between analytical solutions and numerical results is conducted. It could be found that analytical solutions show a good agreement with numerical results.

In the curves of Fig. 7, the variation of pressure and radial displacement is shown. It is obvious that in the first part of elastic deformation, pressure on yieldable steel ribs

Table 2 Geometry, loading and properties of rock and support

Geometry and loading					
Tunnel radius R /m	Initial ground stress p_0/MPa				
4.572	6.895				
Rock parameters					
G^K/MPa	η^K/MPa y	G^M/MPa	η^M/MPa y		
344.738	655.758	3447.379	131183.409		
Support properties					
h/m	E/MPa	v	K_S/MPa	λ_1	λ_2
0.61	16547.420	0.2	2542	0.1	1.0

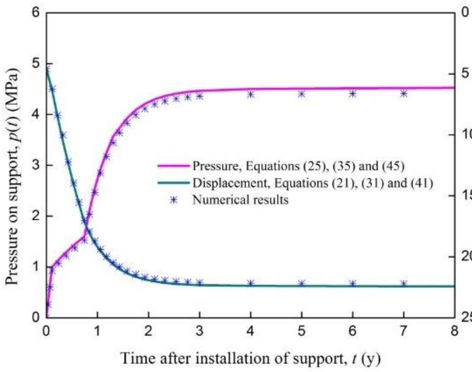

Fig. 7 Pressure and radial displacement of analytical solutions and comparison with numerical results

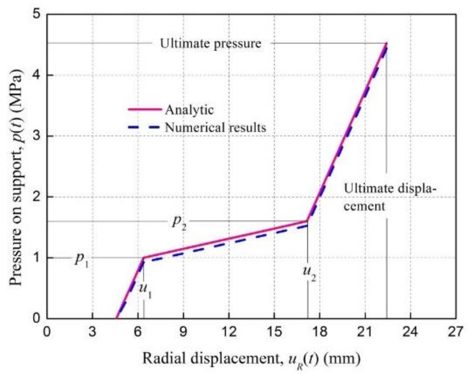

Fig. 8 Support characteristic curve for yieldable steel ribs calculated by theoretical and numerical results after 8 years

increases sharply and it does not take long time to reach the yielding pressure p_1. As the pressure acting on the yieldable steel ribs exceeds the threshold p_1, the support deformation enters the second stage. Because joints of yieldable steel ribs are allowed to slide in the second yielding deformation, yieldable steel ribs are able to accommodate the rock deformation but with small pressure increment in this stage. As illustrated in Fig. 7, displacement also increases rapidly in this stage. By contrast, pressure shows a slowly increasing trend. When shrinkage provided by joints has run out, namely, pressure acting on support has reached critical value p_2, pressure transits to a new increasing stage, as

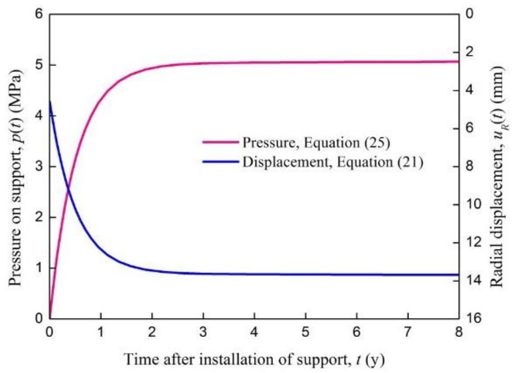

Fig. 9 Pressure and displacement of the Eqs. (21) and (25) without accounting for yielding deformation

shown in Fig. 7. In this stage, pressure grows quickly again due to the sudden change of support stiffness and then growth rate slows down gradually. Finally, pressure enters a steady state.

About the displacement in the rock-support interface, as shown in Fig. 7, during the first and second parts, displacement presents a rapidly increasing trend. Since third part, it is obvious that growth rate of displacement begins to slow down and displacement keeps a constant soon.

As shown in Fig. 8, the principle of pressure-displacement development is well reflected by support characteristic curve. Two lines share the same slope for the same support stiffness in the first and third parts. Pressure grows rapidly with small displacement increment in these two stages. However, the reverse is the case in the second part since weak support stiffness in this stage. So it can also be validated from the Fig. 8 that the yieldable steel ribs are able to accommodate the rock deformation in order to reduce the pressure acting on them.

5.2 Parametric investigation

For the better design of yieldable steel ribs, joints should be paid most attention to. Stiffness correction factor λ_1 and yielding displacement u_2-u_1 are the most important parameters affecting the performance of joints. Based on the analytical solutions provided, a parametric investigation to the influence of joints on supporting effect is performed.

For better comparison, based on the Eqs. (21) and (25), curves for pressure and displacement with time are plotted in Fig. 9, yielding deformation having not been taken into account. The final pressure and displacement after 8 years are expressed as p_c and u_c, respectively.

In the diagrams of Fig. 10(a), the variation of ratio of ultimate pressure p_u considering yielding deformation to p_c with different stiffness correction factors λ_1 is shown. Curves about ratio of ultimate displacement u_u to u_c are displayed in Fig. 10(b). These diagrams are drawn for λ_1=0, 0.05, 0.1, 0.15, 0.2 and (u_2-u_1)/(u_1-u_0)=3.0, 6.0, 9.0, respectively. Remarkably, λ_1=0 could not be submitted to the analytical solutions directly. Here, λ_1=0.001 is suggested to take the place of λ_1=0 to calculate corresponding results.

During joints sliding, the yieldable steel ribs are able to accommodate the rock deformation in order to reduce the pressure acting on them. In this stage, yieldable steel ribs

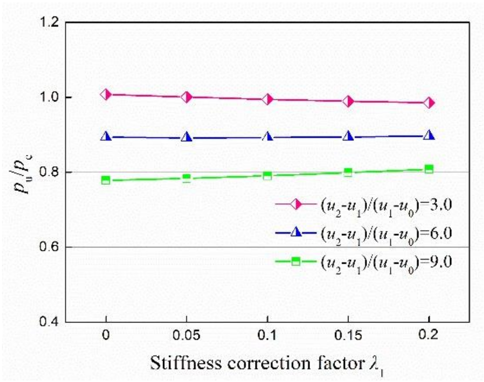

(a) Ultimate pressure p_u

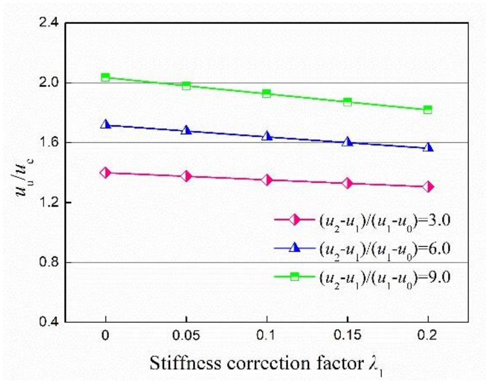

(b) Ultimate displacement u_u

Fig. 10 Ratios of ultimate pressure and displacement considering yielding deformation to p_c and u_c with stiffness correction factor λ_1 after 8 years

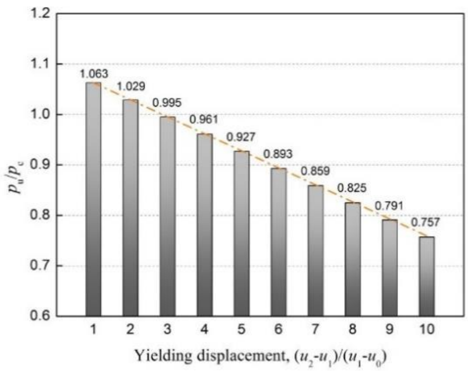

Fig. 11 Ratio of ultimate pressure p_u considering yielding deformation to p_c with different yielding displacements after 8 years

should be seen as the support with weak stiffness. Therefore, taking value of stiffness correction factor λ_1 should be suggested to be small. As shown in Figs. 10(a) and (b), the influence of stiffness correction factor λ_1 on ultimate pressure and displacement could be neglected with it remaining at a low level. But it also could be found from the Figs. 10(a) and (b) that yielding displacement has a great influence on ultimate pressure and displacement. The larger yielding displacement would result in greater ultimate displacement and smaller ultimate pressure. The idea behind all yieldable supports is allowing rock to deform to release rock pressure through over-excavation. The conclusion drawn from Figs. 10(a) and (b) is a good validation for this idea.

In order to investigate the effect of yielding displacement on pressure, Fig. 11 shows the ratios of ultimate pressure p_u considering yielding deformation to p_c with different yielding displacements. The pressure ratios are drawn for λ_1=1 and $(u_2-u_1)/(u_1-u_0)$=1, 2, 3, 4, 5, 6, 7, 8, 9, 10.

As shown in Fig. 11, in linear viscoelastic rock, there is also a linearly descending relationship of pressure with yielding displacement. However, it could also be found from the Fig. 11 that if yielding displacement is not large for a specific type of rheological rock, the reduction of pressure is not obvious, even pressure slightly increases (which may be explained by the inaccuracy of tunnel radius in theoretical derivation). In other words, it is undesirable for yieldable steel ribs to play intended role if yielding displacement is designed to be small. With the gradually increasing of yielding displacement, the pressure linearly decreases. Therefore, it can be concluded that only when the yielding displacement is designed to be large enough could yieldable steel ribs be able to reduce rock pressure without becoming damage through yielding deformation in the second stage. However, it is also never the case that larger yielding displacement certainly results better supporting effect. Because reaction force provided by yieldable steel ribs should also be great enough to avoid loosening damage of rock. For a certain project, the comprehensive investigation on the rock properties, in-situ stress, etc. should be carried out in order to reasonably determine the design of support.

6. Conclusions

Yieldable steel ribs are often recommended in tunnels constructed in rheological rocks. In this paper, mechanical behavior of a circular tunnel supported by yieldable steel ribs in viscoelastic rock is investigated. The following conclusions could be made from the conducted study:

(a) Deformation of yieldable steel ribs can be divided into three stages. Stiffness correction parameters λ_1 and λ_2 are suggested to be introduced to modify the stiffness of yieldable steel ribs in different deformation stages.

(b) Viscoelastic analytical solutions for displacement and pressure in the rock-support interface in the different deformation stages are derived. Yieldable steel ribs are able to reduce the rock pressure without being damaged through the yielding deformation in the second stage.

(c) The influence of stiffness correction factor λ_1 in pressure and displacement could be neglected with it remaining at a low level. But there is a linearly descending relationship of pressure acting on support with yielding displacement in linear viscoelastic rocks.

Acknowledgments

This research is supported by the National Natural

Science Foundation of China (No. 10772143, No. 11872287), the Found of Shaanxi Key Research and Development Program (No. 2019ZDLGY01-10).

References

Cantieni, L. and Anagnostou, G. (2009), "The interaction between yielding supports and squeezing ground", *Tunn. Undergr. Sp. Technol.*, **24**(3), 309-322. https://doi.org/10.1016/j.tust.2008.10.001.

Ding, L.J. and Liu, Y.H. (2018), "Study on deformation law of surrounding rock of super long and deep buried sandstone tunnel", *Geomech. Eng.*, **16**(1), 97-104. https://doi.org/10.12989/gae.2018.16.1.097.

Fan, L.F., Wu, Z.J., Wan, Z. and Gao, J.W. (2017), "Experimental investigation of thermal effects on dynamic behavior of granite", *Appl. Therm. Eng.*, **125**, 94-103. https://doi.org/10.1016/j.applthermaleng.2017.07.007.

Goodman, R.E. (1989), *Introduction to Rock Mechanics* (2th Edition), Willey, New York, U.S.A.

Hu, B., Yang, S.Q. and Xu, P. (2018), "A nonlinear rheological damage model of hard rock", *J. Cent. South Univ.*, **25**(7), 1665-1677.

Huang, H.X., Li, J., Rong, X.L., Hao, Y.Q. and Dong, X. (2017), "A displacement solution for circular openings in an elastic-brittle-plastic rock", *Geomech. Eng.*, **13**(3), 489-504. https://doi.org/10.12989/gae.2017.13.3.489.

Jiang, B.S., Feng, Q., Wang, T. and Liu, Z.Q. (2011), "Mechanical analysis of close type yieldable steel support", *Rock Soil Mech.*, **32**(6), 1620-1642.

Jiao, Y.Y., Song, L, Wang, X.Z. and Adoko, A.C. (2013), "Improvement of the U-shaped steel sets for supporting the roadways in loose thick coal seam", *Int. J. Rock Mech. Min. Sci.*, **60**, 19-25. https://doi.org/10.1016/j.ijrmms.2012.12.038.

Kong, C., Gao, X.Q., Cao, L. and Liu, K. (2016), "Analysis of the failure of primary support of a deep-buried railway tunnel in silty clay", *Eng. Fail. Anal.*, **66**, 259-273. https://doi.org/10.1016/j.engfailanal.2016.04.008.

Lai. J.X., Wang, X.L., Qiu, J.L., Chen, J.X., Hu, Z.N. and Wang, H. (2018), "Extreme deformation characteristics and countermeasures for a tunnel in difficult grounds in southern Shaanxi, China", *Environ. Earth Sci.*, **77**, 706. https://doi.org/10.1007/s12665-018-7888-2.

Lee, Y.J. (2016), "Determination of support pressure under the pile tip using upper and lower bounds with a superimposed approach", *Geomech. Eng.*, **11**(4), 587-605. https://doi.org/10.12989/gae.2016.11.4.587.

Li, X.F., Wang, C.B., Wang, H.L. and Diao, B. (2017), "Experimental study on bearing capacity behavior of U-steel enclosed contractuble support", *J. Zhejiang Univ. Eng. Sci.*, **51**(12), 2355-2364. https://doi.org/10.3785/j.issn.1008-973X.2017.12.007.

Mezger, F., Ramoni, M. and Anagnostou, G. (2018) "Options for deformable segmental lining systems for tunnelling in squeezing rock", *Tunn. Undergr. Sp. Technol.*, **76**, 64-75. https://doi.org/10.1016/j.tust.2017.12.017.

Qiao, R.J., Shao, Z.S., Liu, F.Y. and Wei, W. (2019), "Damage evolution and safety assessment of tunnel lining subjected to long duration fire", *Tunn. Undergr. Sp. Technol.*, **83**, 354-363. https://doi.org/10.1016/j.tust.2018.09.036.

Qiao, R.J., Shao, Z.S., Wei, W. and Zhang, Y.Y. (2018), "Theoretical investigation into the thermo-mechanical behaviours of tunnel lining during RABT fire development", *Arab. J. Sci. Eng.*, **44**(5), 4807-4818. https://doi.org/10.1007/s13369-018-3555-x.

Qiu, J.L., Liu, H.Q., Lai, J.X., Lai, H.P., Chen, J.X. and Wang, K. (2018), "Investigating the long-term settlement of a tunnel built over improved loessial foundation soil using jet grouting technique", *J. Perform. Constr. Fac.*, **32**(5), 04018066. https://doi.org/10.1061/(ASCE)CF.1943-5509.0001155.

Schubert, W. (1996), "Dealing with squeezing conditions in alpine tunnels", *Rock Mech. Rock Eng.*, **29**(3), 145-153. https://doi.org/10.1007/BF01032651.

Sharifzadeh, M., Daraei, R. and Broojerdi, M.S. (2012), "Design of sequential excavation tunneling in weak rocks through findings obtained from displacements based back analysis", *Tunn. Undergr. Sp. Technol.*, **28**, 10-17. https://doi.org/10.1016/j.tust.2011.08.003.

Sharifzadeh, M., Tarifard, A. and Moridi, M.A. (2013), "Time-dependent behavior of tunnel lining in weak rock mass based on displacement back analysis method", *Tunn. Undergr. Sp. Technol.*, **38**, 348-356. https://doi.org/10.1016/j.tust.2013.07.014.

Shin, J.H., Lee, I.M. and Shin, Y.J. (2011), "Elasto-plastic seepage-induced stresses due to tunneling", *Int. J. Numer. Anal. Met.*, **35**(13), 1432-1450. https://doi.org/10.1002/nag.964.

Shin, J.H., Moon, H.G. and Chae, S.E. (2011), "Effect of blast-induced vibration on existing tunnels in soft rocks", *Tunn. Undergr. Sp. Technol.*, **26**(1), 51-61. https://doi.org/10.1016/j.tust.2010.05.004.

Tian, H.M., Chen, W.Z., Tan, X.J., Yang, D.S., Wu, G.J. and Yu, J.X. (2018), "Numerical investigation of the influence of the yield stress of the yielding element on the behavior of the shotcrete liner for yielding support", *Tunn. Undergr. Sp. Technol.*, **73**, 179-186. https://doi.org/10.1016/j.tust.2017.12.019.

Tian, H.M., Chen, W.Z., Yang, D.S., Wu, G.J. and Tan, X.J. (2016), "Numerical analysis on the interaction of shotcrete liner with rock for yielding supports", *Tunn. Undergr. Sp. Technol.*, **54**, 20-28. https://doi.org/10.1016/j.tust.2016.01.025.

Wang, Q., Pan, R., Jiang, B., Li, S.C. He, M.C., Sun, H.B., Wang, L. and Qin, Q. (2017), "Study on failure mechanism of roadways with soft rock in deep coal mine and confined concrete support system", *Eng. Fail. Anal.*, **81**, 155-177. https://doi.org/10.1016/j.engfailanal.2017.08.003.

Wang, T.T. and Huang, T.H. (2014), "Anisotropic deformation of a circular tunnel excavated in a rock mass containing sets of ubiquitous joints: Theory analysis and numerical modeling", *Rock Mech. Rock Eng.*, **47**(2), 643-657. https://doi.org/10.1007/s00603-013-0405-8.

Wu, K. and Shao, Z.S. (2018), "Effects of pipe roof support and grouting pre-reinforcement on the track settlement", *Adv. Civ. Eng.* https://doi.org/10.1155/2018/6041305.

Wu, K. and Shao, Z.S. (2019a), "Visco-elastic analysis on the effects of flexible layer on mechanical behavior of tunnels", *Int. J. Appl. Mech.*, **11**(3), 1950027. https://doi.org/10.1142/S1758825119500273.

Wu, K. and Shao, Z.S. (2019b), "Study on the effect of flexible layer on support structures of tunnel excavated in viscoelastic rocks", *J. Eng. Mech.*, **145**(10), 04019077. https://doi.org/10.1061/(ASCE)EM.1943-7889.0001657.

Wu, K., Shao, Z.S., Qin S. and Li, B.X. (2019), "Determination of deformation mechanism and countermeasures in silty clay tunnel", *J. Perform. Constr. Fac.*, https://doi.org/10.1061/(ASCE)CF.1943-5509.0001381.

Yang, S.Q., Chen, M., Jing, H.W., Chen, K.F. and Meng, B. (2017), "A case study on large deformation failure mechanism of deep soft rock roadway in Xin'An coal mine, China", *Eng. Geol.*, **217**, 89-101. https://doi.org/10.1016/j.enggeo.2016.12.012.

Yang, Y.Z., Shao, Z.S., Mi, J.F. and Xiong, X.F. (2018), "Effect of adjacent hole on the blast-induced stress concentration in rock blasting", *Adv. Civ. Eng.* https://doi.org/10.1155/2018/5172878.

You, C.A. (2002), "Stability analysis of U-steel yieldable support", *Chin. J. Rock Mech. Eng.*, **21**(11), 1672-1675.

Zhao, W.S., Chen, W.Z. and Yang, D.S. (2018), "Interaction between strengthening and isolation layers for tunnels in rock subjected to SH waves", *Tunn. Undergr. Sp. Technol.*, **79**, 121-133. https://doi.org/10.1016/j.tust.2018.05.012.

Zhou, J.F., Xia, Z.Q. and Dan, H.C. (2016), "Theoretical solutions for displacement and stress of a circular opening reinforced by grouted rock bolt", *Geomech. Eng.*, **11**(3), 439-455. https://doi.org/10.12989/gae.2016.11.3.439.

JS